Supplementary information for

Direct Measurement of the Local Glass Transition in Self-Assembled Copolymers with Nanometer Resolution

Dane Christie[1], Richard A. Register[1,2*], and Rodney D. Priestley[1,2*]

***Correspondence to:** register@princeton.edu and rpriestl@princeton.edu

Supplementary Text

Molecular Characterization

Table S1: Molecular weight, dispersity, and PMMA weight and volume fractions for the labeled homopolymers and copolymers employed in this work. The volume fractions (at 438 K) were calculated assuming that the blocks have specific volumes identical to those of the corresponding homopolymer. The values of the homopolymer densities are 1.13 g/mL and 0.97 g/mL at 438 K for PMMA and PBMA respectively[44].

Polymer	Mw (kg/mol)	Đ	Mn (kg/mol)	w_{PMMA}	ϕ_{PMMA}
PMMA-py homopolymers					
PMMA	3.5	1.10	3.2	1	1
PMMA	8.8	1.05	8.4	1	1
PMMA	37	1.07	34	1	1
PMMA	73	1.07	69	1	1
PMMA	153	1.10	139	1	1
PBMA-py homopolymers					
PBMA	84	1.09	75	0	0
Lamellar PBMA-PMMA diblock copolymers					
PBMA-PMMA-U	47	1.06	45	0.53	0.49
PBMA-PMMA-E	49	1.07	46	0.56	0.52
PBMA-PMMA-J	47	1.06	45	0.55	0.51
PBMA-PMMA-5	64	1.10	58	0.56	0.52
PBMA-PMMA-20	56	1.10	51	0.56	0.52
PBMA-PMMA-50	52	1.09	47	0.54	0.50
PBMA-U-PMMA	58	1.05	55	0.55	0.51
PBMA-E-PMMA	73	1.04	70	0.56	0.52
PBMA-J-PMMA	73	1.04	70	0.53	0.49
PBMA-5-PMMA	59	1.05	56	0.54	0.50
PBMA-20-PMMA	52	1.05	50	0.55	0.51
PBMA-50-PMMA	54	1.04	52	0.55	0.52
PBMA-PMMA-U	26	1.05	25	0.55	0.51
PBMA-PMMA-E	28	1.06	27	0.55	0.52
PBMA-PMMA-J	27	1.05	26	0.56	0.52
PBMA-PMMA-5	28	1.06	26	0.55	0.52
PBMA-PMMA-20	25	1.05	24	0.55	0.51
PBMA-PMMA-50	30	1.05	29	0.57	0.54
Homogeneous PBMA-PMMA diblock copolymers					
PBMA-PMMA-50/50	16.1	1.05	15.3	0.55	0.51
PBMA-PMMA-40/60	18.3	1.08	16.9	0.60	0.56
PBMA-PMMA-30/70	16.6	1.04	16.0	0.63	0.59
PBMA-PMMA-20/80	18.8	1.04	18.1	0.76	0.73
PBMA-PMMA-10/90	15.8	1.05	15.0	0.87	0.85
PBMA-PMMA-5/95	18.0	1.04	17.3	0.94	0.93

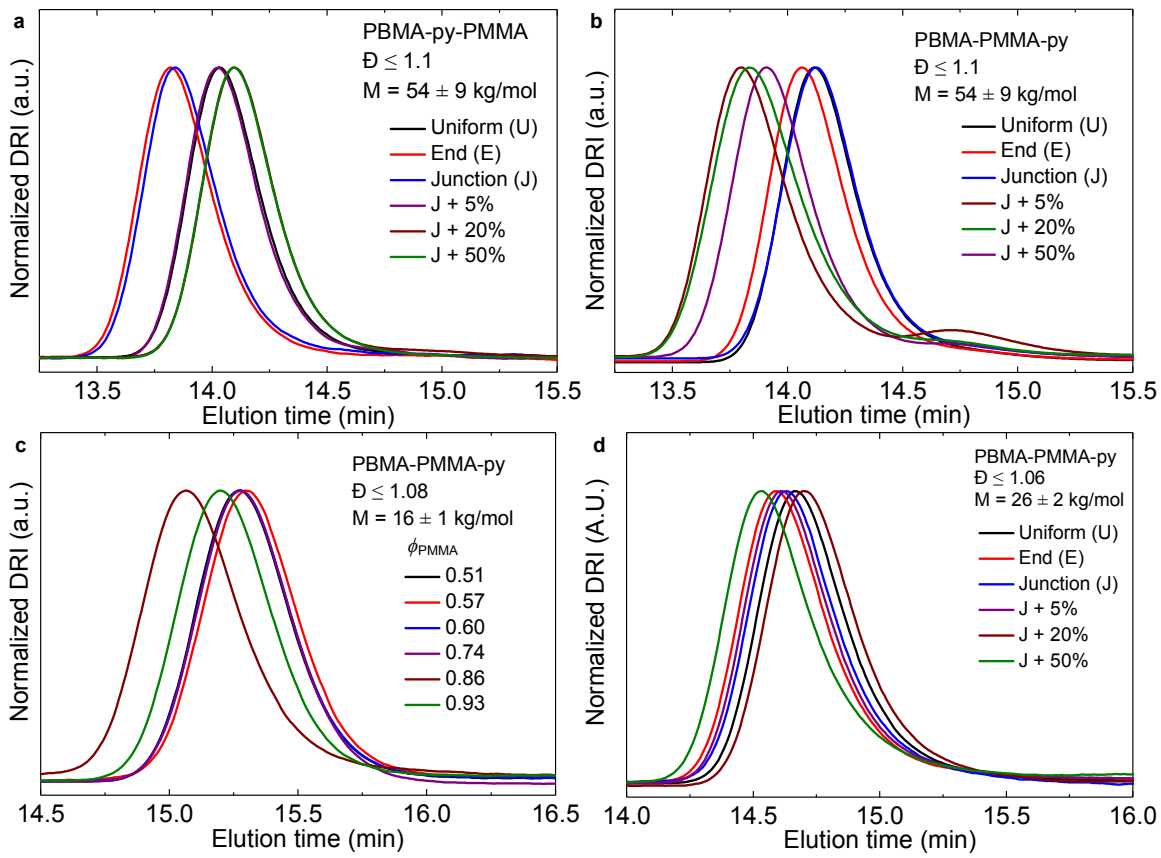

Figure S1: GPC traces of two series of labeled lamella-forming PBMA-PMMA diblock copolymers, where the pyrene-bearing monomer was incorporated into a) the PBMA block, or b) the PMMA block. c) GPC traces of a series of labeled PBMA-PMMA diblock copolymers which form homogeneous melts, where the pyrene-bearing monomer was randomly distributed along the PMMA block. d) GPC traces of a series of labeled lamella-forming PBMA-PMMA diblock copolymers, where the pyrene-bearing monomer was incorporated into the PMMA block.

Randomness of Pyrene Incorporation

To investigate the randomness of incorporation of the pyrene-bearing monomers within a labeled segment, a statistical copolymerization of methyl methacrylate and 1-pyrenylbutyl methacrylate (0.8 mol% of monomer charge) was run under the same conditions used for polymerization. Two identical reactions were run in parallel, one terminated at 45 sec (partial monomer conversion) and one terminated at 10 min (full conversion). Figure S2 displays GPC traces of the products of the reactions terminated at 45 sec (M = 24 kg/mol) and 10 minutes (M = 69 kg/mol), showing both the DRI and UV absorbance (λ = 340 nm) signals. The absorbance signal at 340 nm comes solely from the pyrene units on the chain.

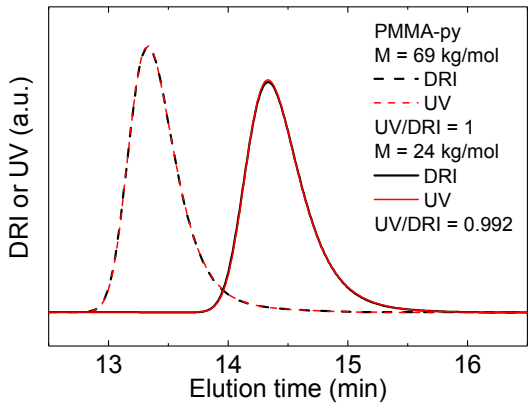

Figure S2: GPC traces for the products of identical pyrene-labeled PMMA homopolymer syntheses terminated at partial conversion (45 sec after monomer addition, M = 24 kg/mol) and full conversion (10 min, M = 69 kg/mol), showing both the differential RI and UV absorbance (λ = 340 nm) signals.

The ratio of the integrated UV and DRI signals, UV/DRI (proportional to the absorbance per unit polymer mass) serves as a proxy for the relative incorporation of pyrene at low conversion vs. complete conversion, and is normalized to unity at complete conversion (10 min reaction). For the 45 sec reaction, with a conversion of 24/69 = 0.35, the UV/DRI ratio was measured as 0.992, indicating no significant drift of pyrene content over time. Note that this experiment was carried out by instantaneously charging the reactor with all of the monomer mixture; however, for all the polymers synthesized to characterize T_g in this work, the monomer mixture was added dropwise over a period of 1 - 2 minutes, further minimizing the already insignificant composition gradient within the labeled section.

<u>T_g Characterization: Fluorimetry</u>

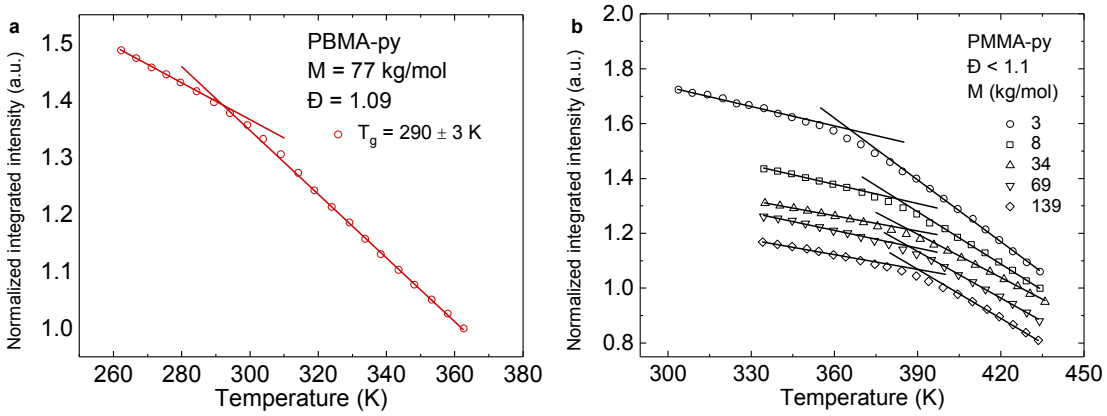

Figure S3: Fluorescence characterization of PMMA and PBMA homopolymers. a) Normalized integrated intensity vs. temperature for a pyrene-labeled PBMA homopolymer (M = 77 kg/mol, Đ = 1.09). b) Normalized integrated intensity vs. temperature for a series of pyrene-labeled PMMA homopolymers. Each curve

was normalized to a value of unity at the highest temperature of data collection and then shifted vertically for clarity.

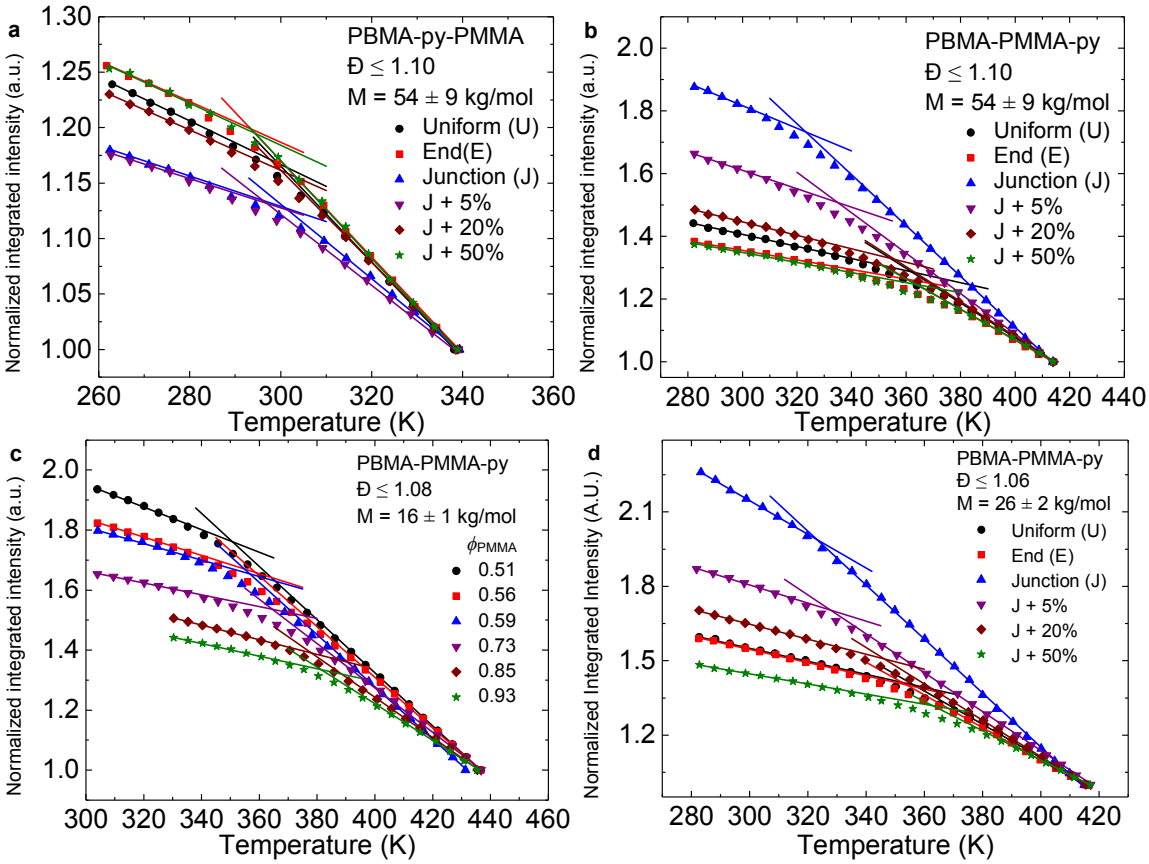

Figure S4: Fluorescence characterization of PBMA-PMMA diblock copolymers. a) Temperature dependence of the integrated fluorescence emission intensity and the corresponding linear fits for the series of selectively labeled, near-symmetric PBMA-PMMA diblock copolymers with $\chi N/(\chi N)_{ODT}$ = 2.4. Pyrene was incorporated at various positions along the PBMA block. b) Temperature dependence of the integrated fluorescence emission intensity and the corresponding linear fits for the analogous $\chi N/(\chi N)_{ODT}$ = 2.4 with pyrene incorporated at various positions along the PMMA block. c) Temperature dependence of the integrated fluorescence emission intensity and the

corresponding extrapolated linear fits in the glassy and rubbery regions of PBMA-PMMA diblock copolymers (M = 16 ± 1 kg/mol) of different compositions. Pyrene was randomly distributed throughout the PMMA block. d) Temperature dependence of the integrated fluorescence emission intensity and the corresponding linear fits for the series of weakly segregated, selectively labeled, near symmetric PBMA-PMMA diblock copolymers with $\chi N/(\chi N)_{ODT}$ = 1.2. Pyrene was incorporated at various positions along the PMMA block.

T_g Characterization: DSC

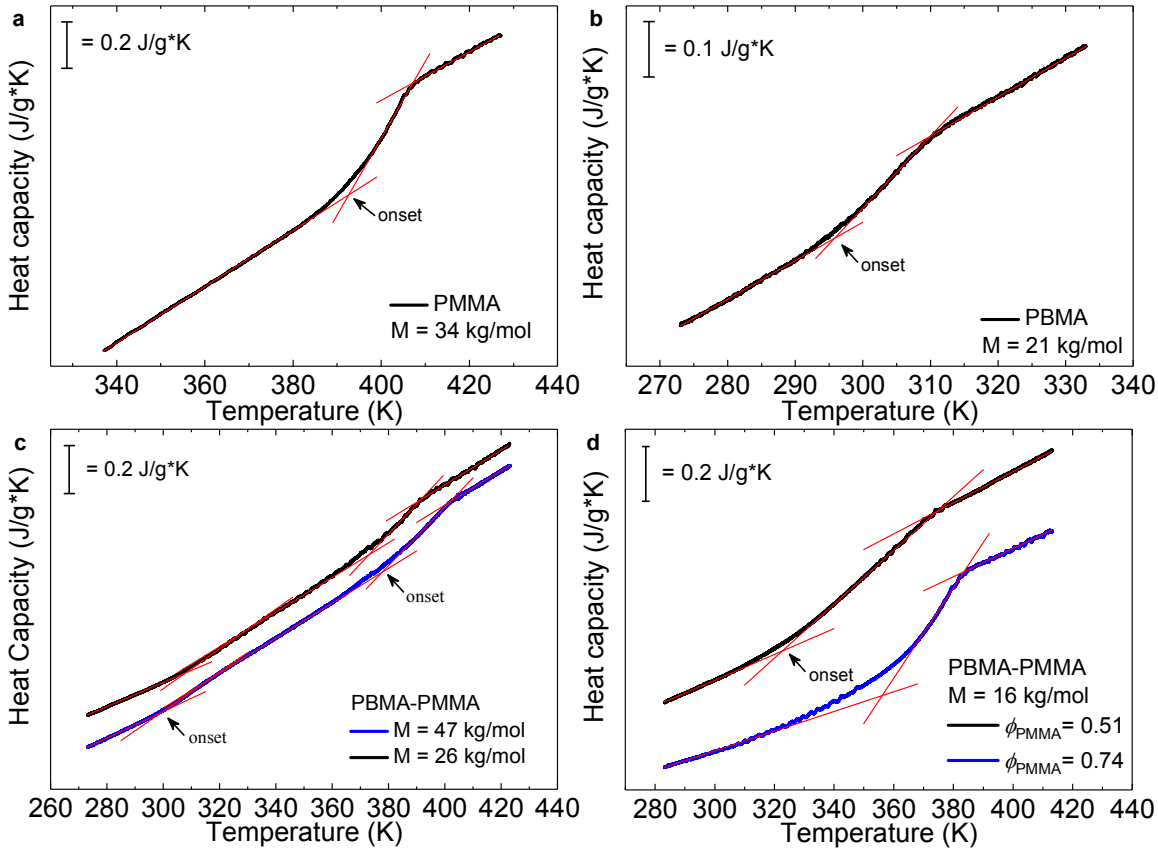

Figure S5: DSC characterization of PBMA and PMMA homopolymers, and PBMA-PMMA diblock copolymers. a) Thermogram (black) of a PMMA

homopolymer with linear fits to the data (red) in the glassy, rubbery, and transition regions of the curve. The intersections of the lines represent the onset and endpoint of the glass transition, with the onset indicated in the graph. b) Thermogram of a PBMA homopolymer. c) Thermograms of two lamellar PBMA-PMMA diblock copolymers (M = 47 kg/mol, ϕ_{PMMA} = 0.51 and M = 26 kg/mol, ϕ_{PMMA} = 0.52). d) Thermograms of two homogeneous PBMA-PMMA diblock copolymers (M = 16 $\pm$ 1 kg/mol) with different values of ϕ_{PMMA}.

Table S2: T_g as determined by DSC for an unlabeled PBMA homopolymer (M = 21 kg/mol, Đ = 1.07), a labeled PMMA homopolymer (M = 34 kg/mol, Đ = 1.07), a labeled lamella-forming diblock copolymer of PBMA-PMMA (PBMA-U-PMMA: M = 55 kg/mol, ϕ_{PMMA} = 0.51), and a labeled lamella-forming diblock copolymer of PBMA-PMMA (PBMA-PMMA-5 : M = 26 kg/mol, ϕ_{PMMA} = 0.52). $\Delta T_g = T_{g,endpoint} - T_{g,onset}$.

Polymer	**$T_{g,onset}$ (K)**		**ΔT_g (K)**	
PBMA	296		14	
PMMA	392		12	
PBMA-U-PMMA	301	382	15	20
PBMA-PMMA-5	304	374	15	20

Estimation of χN

Within the framework of self-consistent field theory, the phase diagram of a diblock copolymer is constructed as the product of the Flory interaction

parameter (χ) between the two blocks and the total degree of polymerization (N) of the diblock copolymer versus the volume fraction (ϕ) of one block[12]. Temperature-dependent SAXS measurements on a series of unlabeled lamellar diblock copolymers of PBMA-PMMA, whose GPC traces are shown in Fig. S6a, were performed in order to estimate χN. The range of polymer molecular weights synthesized was based on previous literature[45], in order to span the order-disorder transition (ODT). Fig. S6b shows the temperature-dependent absolute scattering intensity of a 22 kg/mol, near-symmetric PBMA-PMMA diblock copolymer (ϕ_{PMMA} = 0.48). This diblock copolymer exhibited an ODT temperature, T_{ODT} = 456 ± 1 K, as noted by a sharp decrease in the full width at half maximum (FWHM) of the absolute scattering intensity upon cooling from the disordered melt as plotted in Fig. S6c.

$$(\chi N)_{ODT} = 10.5 + 41\bar{N}^{-1/3} + 123\bar{N}^{-0.56} \qquad \text{(S1)}$$

Based on this observation, and the value of χN = 18.4 at the ODT for a symmetric diblock copolymer determined within the framework of renormalized one-loop (ROL) theory[46], see equation (S1), χN was estimated for all of our polymers (at temperatures in the vicinity of 456 K) as χN =18.4 × (M/22 kg/mol). Equation S1 is a fluctuation correction to the value of $(\chi N)_{ODT}$ = 10.5 originally predicted by Leibler[47] for a symmetric diblock. The invariant degree of polymerization ($\bar{N} = N(cb^3)^2$) is a measure of overlap between a reference chain and the remaining chains in the system; c = 5.1 nm^{-3} is the inverse monomer volume calculated for the diblock copolymer from the volume fraction-weighted homopolymer melt density at the ODT (T = 456 K) and b = 0.72 nm is the

average statistical segment length reported in the literature for a near-symmetric PBMA-PMMA diblock copolymer[45]. The values of $\bar{N}$ for diblock copolymers at the ODT and weak segregation are 661 and 766, respectively. Two other polymers for which GPC traces are presented in Fig. S6a were either ordered over the entire range of observation, up to T = 468 K (M = 26 kg/mol, ϕ_{PMMA} = 0.52), or disordered over the entire range of observation, down to T = 423 K (M = 18 kg/mol, ϕ_{PMMA} = 0.52).

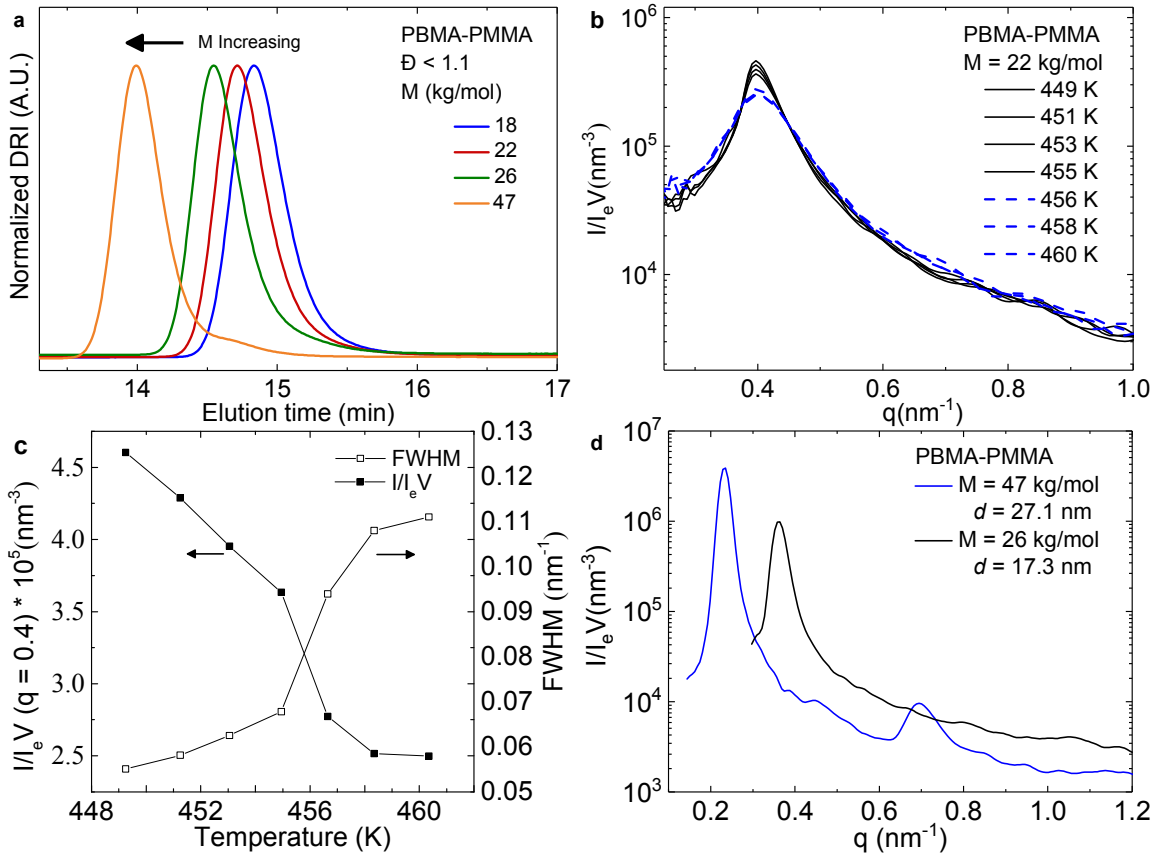

Figure S6: Characterization of PBMA-PMMA diblock copolymers. a) GPC traces of a series of lamella-forming diblock copolymers of PBMA-PMMA. b) Temperature-dependent SAXS profiles of a near-symmetric diblock copolymer of PBMA-PMMA (M = 22 kg/mol, Đ = 1.07, ϕ_{PMMA} = 0.48). c) Temperature-

dependent peak intensity and FWHM from the SAXS profiles in Fig. S6b, indicating T_{ODT} = 456 ± 1 K. d) SAXS profile of a lamella-forming unlabeled PBMA-PMMA diblock copolymer (M = 47 kg/mol, Đ = 1.06, ϕ_{PMMA} = 0.53) at T = 438 K, whose GPC trace is shown in Fig. S6a, and a labeled PBMA-PMMA diblock copolymer (M = 26 kg/mol, Đ = 1.06, ϕ_{PMMA} = 0.52) at T = 438 K.

SAXS measurements were also used to determine the diblock copolymer domain period ($d = 2\pi/q^*$) and the thickness of the polymer-polymer interface (*t*). A graphical illustration of *t* is shown in Fig. S7d. A representative melt SAXS pattern of an unlabeled PMMA-PBMA diblock copolymer (M = 47 kg/mol) is shown in Fig. S6d, where *d* = 27.1 nm. The interfacial thickness was extracted from[48] equation (S2):

$$I_n \sim n^{-4}(\rho_A - \rho_B)^2[sin^2(n\pi\phi_A)]e^{-kn^2} \qquad \text{(S2)}$$

which relates the integrated scattering intensity of the nth-order reflection to the electron density contrast ($\rho_A - \rho_B$) and the volume fraction (ϕ_A) of a component in the diblock, where $k = 2\pi\,(t/d)^2$; by taking the ratio of the integrated intensities of the two odd-order peaks[49] in Fig. S6d, I_1/I_3 = 260, a value of *t* = 3.8 nm was calculated.

Composition profiles

The primary motivation for performing a fluctuation correction to the values of χN according to equation (S1), is to obtain the most accurate composition profiles possible for use in calculating T_g based on the LM model. In

the vicinity of the ODT, the composition profiles as determined by SCFT are more weakly segregated than observed in experiments[43]. This trend is most prominent at the ODT where the composition profile based on SCFT is flat, while the composition profile at the ODT based on ROL, as shown in Figure S7a, has a large amplitude. Fluctuation-corrected composition profiles for both the weak (M = 26 kg/mol) and intermediate (M = 54 kg/mol) segregation strength diblock copolymers were determined as described below.

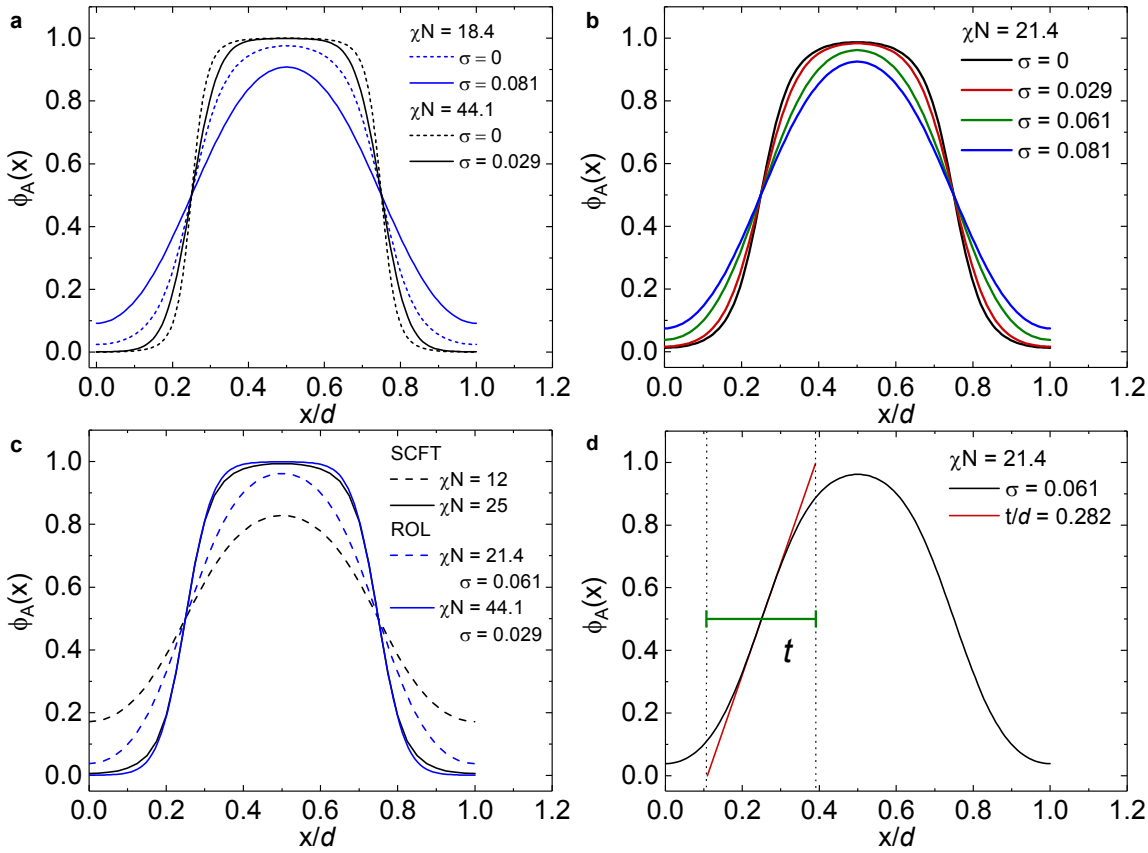

Figure S7: a) Unsmeared (dashed lines) and smeared (solid lines) composition profiles of block A at the ODT (blue lines) and at intermediate segregation strength (black lines). b) Composition profiles at weak segregation strength smeared by the value of σ at the ODT (σ = 0.081), the value of σ calculated for

this polymer based on the results of Medapuram et al. (σ = 0.061), or the value of σ for the diblocks of intermediate segregation strength (σ = 0.029). c) Composition profiles at weak and intermediate segregation strengths as determined by SCFT (black lines) or ROL (blue lines). d) Interfacial thickness of a lamellar diblock copolymer at χN = 21.4 smeared by σ = 0.061; *t* is determined by evaluating the first derivative of the composition profile at the domain interface.

The interfacial thickness of the weakly segregated diblock copolymer (χN = 21.4) cannot be extracted from the SAXS trace in Figure S6d due to the absence of higher-order reflections. *t* is estimated from the fluctuation-corrected composition profile according to a procedure described by Medapuram et al.[46] For any value of χN the corresponding SCFT composition profile represents an intrinsic profile (ϕ^{int}) which is more strongly segregated than the average and contains no fluctuations.

$$\phi_A(z) = \int dh \phi^{(int)}(z+h)P(h) \quad \text{(S3)}$$

The average profile, see equation (S3), is given by a convolution approximation where monomer segments undergo a displacement, *h*, normal to the interface and is weighted by a Gaussian probability distribution where $\langle h^2 \rangle \equiv \sigma^2$. The displacement at the ODT, σ_{ODT} = 0.081, is determined by smearing the profile until the concentration in the center of the domain is equal to 0.908 as observed by Medapuram et al. for $\bar{N}$ = 661 and is plotted in Figure S7a. The profiles at intermediate segregation strength (χN = 44.1) are smeared by a displacement, σ_{SAXS} = 0.029, selected to match the interfacial thickness, *t* = 3.8

nm, as determined by SAXS; this composition profile is also plotted in Figure S7a.

Figure S7b plots the composition profile of the weakly segregated polymer after applying various values of the displacement: σ = 0 (the intrinsic profile), σ = 0.081 (the value at the ODT), σ = 0.029 (the value at intermediate segregation strength), and σ = 0.061 (selected to match the ratio of the first and third coefficients (A_3/A_1) of a Fourier expansion representation of the composition profile for a weakly segregated diblock copolymer whose $\bar{N}$ = 766, was interpolated between values of $\bar{N}$ = 480 and 960 provided by Medapuram et al.[46]). The profile for the weakly segregated diblock copolymer smeared by σ = 0.061 provides the basis for estimating the interfacial thickness, monomer positions, and local T_g using the LM model for the weakly segregated diblock copolymer, Fig. S7d.

For comparison, the effect of fluctuation corrections to the composition profiles are shown in Fig. S7c. At intermediate segregation strength, the difference between the profiles as calculated by SCFT or ROL is negligible. In contrast, there is a dramatic difference between the profiles determined by SCFT or ROL at weak segregation strength: the former has a much larger interfacial thickness and smaller volume fraction of block A in the center of the domain than the latter.

Estimation of ϕ_s

The value of the self-concentration fraction (ϕ_s) can be estimated according to equation (S4), where C_∞ is the characteristic ratio, m_0 the repeat unit molar mass, a the number of backbone bonds per repeat unit, ρ the density, N_{av} Avogadro's number, and V the volume occupied by Kuhn length's worth of monomers[23].

$$\phi_s = \frac{C_\infty m_0}{a\rho N_{av} V} \qquad \text{(S4)}$$

Lodge and coworkers approximated V as the volume of a cube whose length is that of a Kuhn segment, but the exact value of ϕ_s could vary from that given in eqn. (S4) by a factor of order unity. By eqn. (S4), $\phi_{s,PMMA}$ = 0.25 is calculated[23]; in the present work, $\phi_{s,PMMA}$ = 0.38 was extracted from the fit of the fluorescence T_g vs. ϕ_{PMMA} data for homogeneous PBMA-PMMA diblock copolymers shown in Fig. 1d. For PBMA, ϕ_s = 0.5 was calculated according to eqn. (S4), where the Kuhn segment length $b = C_\infty l$ and l is the length of a backbone bond (1.54 Å). The value of C_∞ used for PBMA was 8.0[50].

Effective composition profiles and local T_g

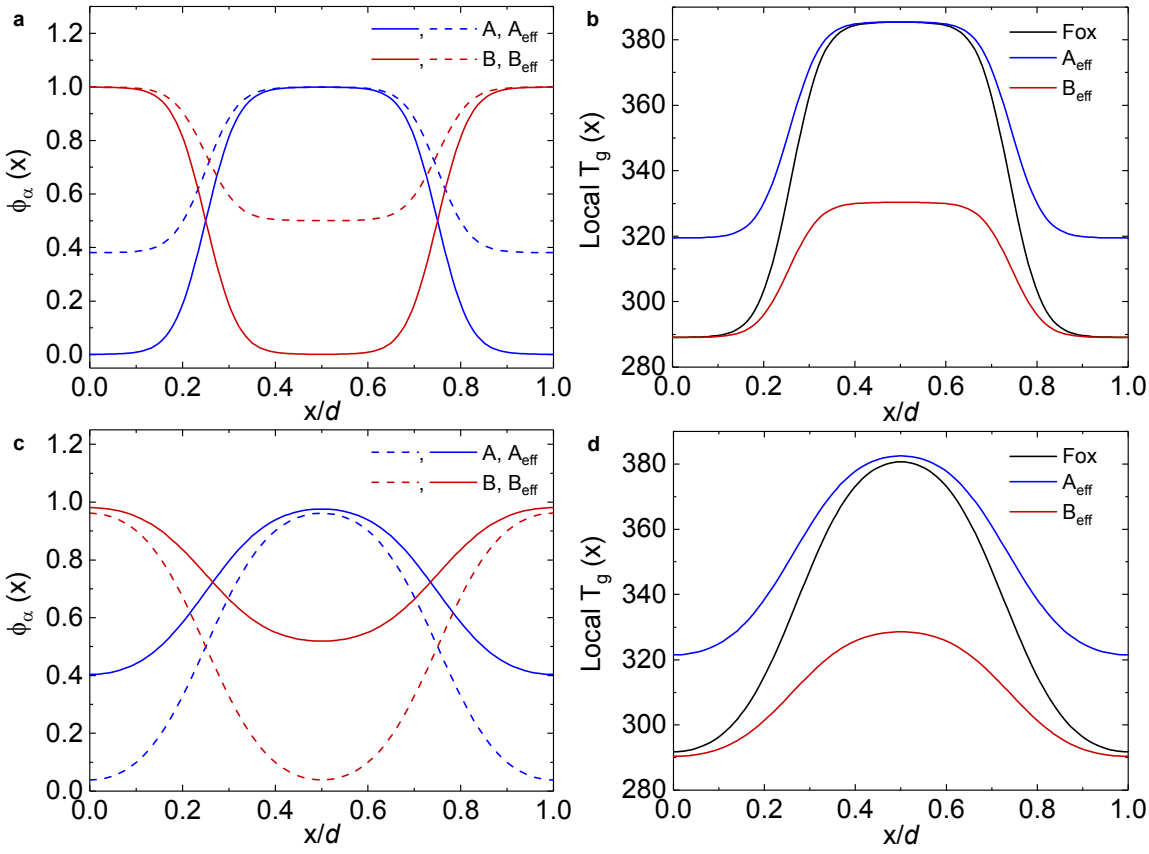

Figure S8: Effective composition and T_g profiles for a PBMA-PMMA diblock copolymer. a) Composition (solid) and effective composition (dashed) profiles of a symmetric diblock copolymer of intermediate segregation strength (χN = 44.1; $\chi N/(\chi N)_{ODT}$ = 2.4, σ = 0.029) where $\phi_{s,A}$ = 0.38 and $\phi_{s,B}$ = 0.5. The effective composition (ϕ_{eff}) profile is that experienced locally by an A or B segment in the diblock, accounting for self-concentration. b) Corresponding T_g profiles for the same symmetric diblock copolymer (χN = 44.1) as calculated by the Fox equation, with the composition given either by the smeared SCFT (ROL) profile ("Fox"), or after accounting for self-concentration, as experienced locally by the A

and B segments ("A_{eff}", "B_{eff}"). The homopolymer T_g values of 385 K and 289 K for blocks A (PMMA) and B (PBMA) were employed with self-concentration fractions of $\phi_{s,A}$ = 0.38 and $\phi_{s,B}$ = 0.5. c) Composition (solid) and effective composition (dashed) profiles of a symmetric diblock copolymer of weak segregation strength (χN = 21.4; $\chi N/(\chi N)_{ODT}$ = 1.2, σ = 0.061) where $\phi_{s,A}$ = 0.38 and $\phi_{s,B}$ = 0.5. The effective composition (ϕ_{eff}) profile is that experienced locally by an A or B segment in the diblock, accounting for self-concentration. d) Corresponding T_g profiles for the same symmetric diblock copolymer (χN = 21.4) as calculated by the Fox equation, with the composition given either by the smeared SCFT profile ("Fox"), or after accounting for self-concentration, as experienced locally by the A and B segments ("A_{eff}", "B_{eff}"). The homopolymer T_g values of 385 K and 289 K for blocks A (PMMA) and B (PBMA) were employed with self-concentration fractions of $\phi_{s,A}$ = 0.38 and $\phi_{s,B}$ = 0.5.

Validity of linearly weighting the local T_g by the monomer segment distribution

In Figures 4 and 5, the average segment position is represented by a simple linear weighting of the segment position by the composition profile (i.e., by the fraction of labeled segments located at a particular value of x); similarly, in the LM model calculations, the T_g value was represented by the linear weighting over the T_g profiles of Fig. S8b and Fig. S8d. The adequacy of this linear weighting is demonstrated by a comparison with the T_g measured for the diblocks uniformly labeled over their PMMA blocks (PBMA-PMMA-U, at both intermediate and weak segregation). The calculated composition profiles for selectively-

labeled diblocks (Fig. 3 and S11) were summed together, with adjustable weights, in order to accurately represent the segment density profiles calculated for the U-labeled diblocks.

These same weights were then applied to the T_g values to estimate T_g for each U-labeled diblock, which could be compared with experiment. The segment density distributions are shown in Fig. S9; for the χN = 44.1 diblock, the sum represented the U-labeled profile to within 3% at any value of x, while for the χN = 21.4 diblock, the agreement was within 0.9%. The weights are given in Table S3. For the χN = 44.1 diblock, the T_g value obtained by summation was 359 K, vs. 362 K measured by experiment; for the χN = 21.4 diblock, the T_g value obtained by summation was 353 K, vs. 352 K measured by experiment. In both cases, the calculated and measured values agree to within the error of T_g determination by fluorescence.

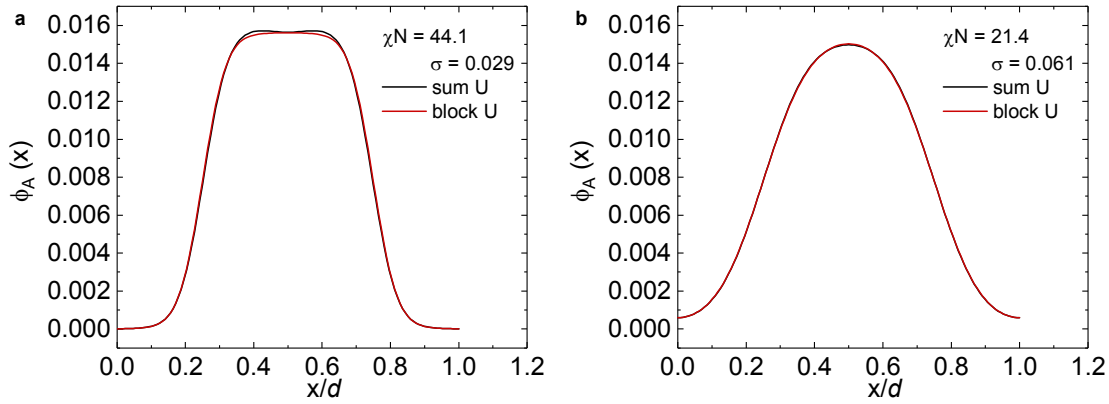

Figure S9: a) Normalized composition profiles of block A calculated at χN = 44.1, and σ = 0.029, and by summation of the selectively-labeled monomer segments. b) Normalized composition profiles of block A calculated at χN = 21.4,

and σ = 0.061, or by summation of the selectively-labeled monomer segments. All curves are normalized by their respective areas.

Table S3: Experimental T_g of labeled monomer segments and the respective weights used to calculate the value of the U-labeled diblock copolymer as described above.

Label position	**$T_{g,label}$ (K) for χN =**		**Weight for χN =**	
	44.1	**21.4**	**44.1**	**21.4**
Junction (J)	322	323	0.02	0.02
J + 5%	334	327	0.05	0.07
J + 20%	354	346	0.25	0.23
J + 50%	364	362	0.33	0.46
End (E)	364	353	0.35	0.22

Monomer segment position

Amongst a variety of potential choices, the position of a monomer segment relative to the interface could be represented by the peak of the distribution or by the composition-weighted average, as shown in Fig. S10a. In Fig. S10b, the peak and average positions of labeled monomer segments are plotted for different values of χN. The average position displays a trend where all monomer segments converge to x/*d* = 0.25 as χN approaches 10.5, since at the ODT (χN = 10.5), the composition distribution for all segments is flat

(independent of x/*d*). The peak of the monomer segment distribution, also shown in Fig. S10b, displays a dissimilar trend, implying that the peak position is a poor choice to represent the label's x/*d*.

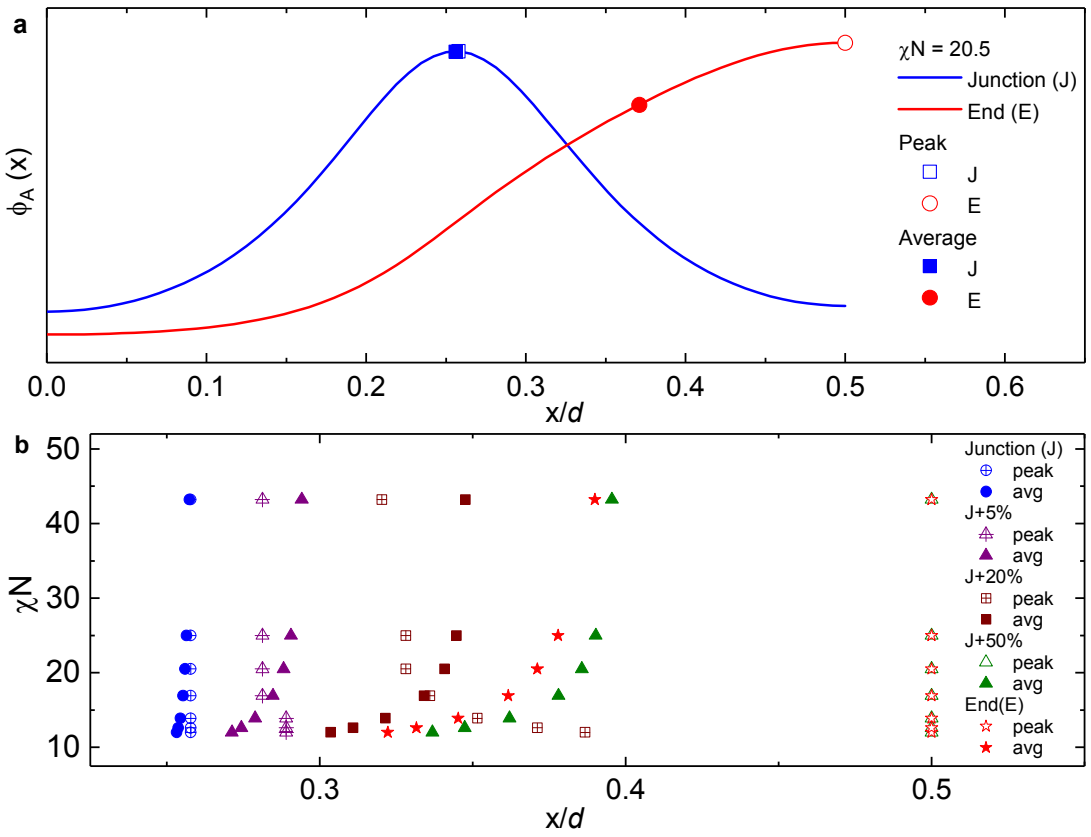

Figure S10: a) Unsmeared composition profile of end or junction monomer segments of block A at χN = 20.5, presented to illustrate the difference between the peak (open symbols) and the average (closed symbols) of the distributions. b) Monomer segment position as represented by the peak (open symbols) or average (solid symbols) of the distribution for different values of χN, as calculated from SCFT (no ROL correction).

Monomer segment distribution: weakly segregated diblock copolymer

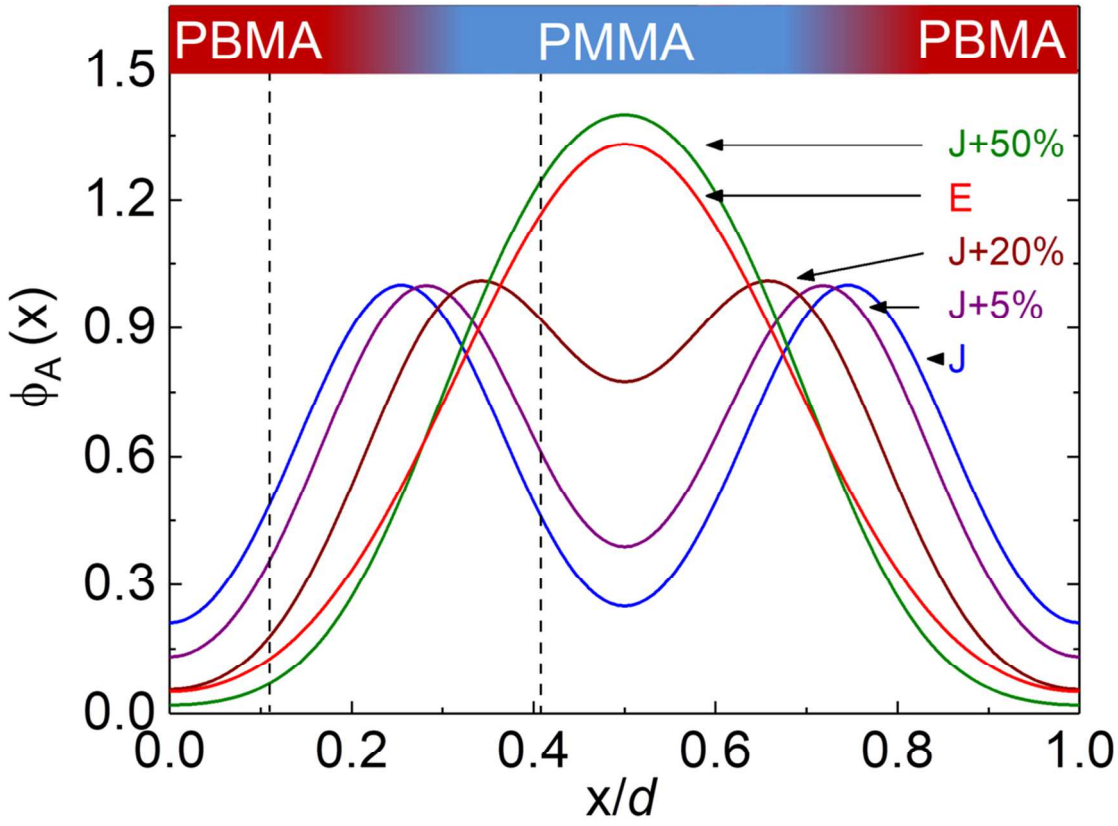

Figure S11: Composition profile of labeled segments across the domain period (*d*) of a symmetric diblock copolymer where $\chi N/(\chi N)_{ODT}$ = 1.2, for the five different label positions schematized in Figure 2a. Profiles have been smeared with a displacement σ = 0.061. Dashed vertical lines demarcate the width of the interface as determined in Fig S7d. Profiles are normalized to equal area, with the highest value of the junction-labeled segment density (ϕ_A) set to unity.

References:

44. Orwoll, R. A. Densities, Coefficients of Thermal Expansion, and Compressibilities of Amorphous Polymers. In *Physical properties of polymers handbook*, 2nd ed.; Mark, J. E., Ed.; Springer Science+Business Media: New York, (2007).

45. Scherble, J.; Stark, B.; Stühn, B.; Kressler, J.; Budde, H.; Höring, S.; Schubert, D.; Simon, P.; Stamm, M. Comparison of interfacial width of block copolymers of d_8-poly (methyl methacrylate) with various poly (n-alkyl methacrylate)s and the respective homopolymer pairs as measured by neutron reflection. *Macromolecules* **1999,** *32*, 1859-1864.

46. Medapuram, P.; Glaser, J.; Morse, D. C. Universal Phenomenology of Symmetric Diblock Copolymers near the Order–Disorder Transition. *Macromolecules* **2015**, *48*, 819-839.

47. Leibler, L. Theory of microphase separation in block copolymers. *Macromolecules* **1980,** *13*, 1602-1617.

48. Roe, R.-J. *Methods of X-ray and neutron scattering in polymer science*. Oxford University Press, New York, (2000).

49. Beckingham, B. S.; Register, R. A. Architecture-induced microphase separation in nonfrustrated A-B-C triblock copolymers. *Macromolecules* **2013**, *46*, 3486-3496.

50. Wu, S. Control of intrinsic brittleness and toughness of polymers and blends by chemical structure: a review. *Polym. Int.* **1992**, *29*, 229-247.